Journal of Molecular Modeling (2022) 28:80
https://doi.org/10.1007/s00894-022-05046-6

ORIGINAL PAPER

A descriptor for the structural stability of organic–inorganic hybrid perovskites based on binding mechanism in electronic structure

Xiaoshuo Liu[1,2] · Yang Bai[1] · Shengyi Chen[1] · Chongchong Wu[3] · Ian D. Gates[3] · Tianfang Huang[2] · Wei Li[4,5] · Weijie Yang[1] · Zhengyang Gao[1] · Jianxi Yao[6,7] · Xunlei Ding[4,5]

Received: 17 February 2021 / Accepted: 31 January 2022

Abstract

The poor stability of organic–inorganic hybrid perovskites hinders its commercial application, which motivates a need for greater theoretical insight into its binding mechanism. To date, the binding mode of organic cation and anion inside organic–inorganic hybrid perovskites is still unclear and even contradictory. Therefore, in this work based on density functional theory (DFT), the binding mechanism between organic cation and anion was systematically investigated through electronic structure analysis including an examination of the electronic localization function (ELF), electron density difference (EDD), reduced density gradient (RDG), and energy decomposition analysis (EDA). The binding strength is mainly determined by *Coulomb effect* and orbital polarization. Based on the above analysis, a novel 2D linear regression descriptor that $E_b = -9.75Q^2/R_0 + 0.00053\ V \bullet E_{HL} - 6.11$ with coefficient of determination $R^2 = 0.88$ was proposed to evaluate the binding strength (the units for Q, R_0, V, and E_{HL} are |e|, Å, bohr^3, and eV, respectively), revealing that larger *Coulomb effect* (Q^2/R_0), smaller volume of perovskite (V), and narrower energy difference (E_{HL}) between the lowest unoccupied molecular orbital (LUMO) of organic cation and the highest occupied molecular orbital (HOMO) of anion correspond to the stronger binding strength, which guides the design of highly stable organic–inorganic hybrid perovskites.

Keywords Density functional theory · Organic–inorganic hybrid perovskites · Binding energy · Structural stability · Goldschmidt tolerance factor

Introduction

Since the proposed use of perovskite-based solar cells (PSCs) by Kojima et al. in 2009 [1], studies on PSCs have attracted extensive attention. Recently, organic–inorganic hybrid perovskites, represented by $MAPbI_3$ ($MA^+ = CH_3NH_3^+$, methylammonium), have become super absorbent materials for solar cells with advantages of easy synthesis, tunable optical band gaps, and great power conversion efficiency (PCE) [2]. The theoretical maximum PCE of the traditional silicon solar cell is ~ 29% [3], and nowadays, as a promising

✉ Zhengyang Gao
gaozhyan@163.com

✉ Jianxi Yao
jianxiyao@ncepu.edu.cn

✉ Xunlei Ding
dingxl@ncepu.edu.cn

1 Department of Power Engineering, School of Energy, Power, and Mechanical Engineering, North China Electric Power University, Baoding 071000, China

2 Key Laboratory of Energy Thermal Conversion and Control of Ministry of Education, School of Energy and Environment, Southeast University, Nanjing 210096, China

3 Department of Chemical and Petroleum Engineering, University of Calgary, Calgary, AB T2N 1N4, Canada

4 School of Mathematics and Physics, North China Electric Power University, Beijing 102206, China

5 Institute of Clusters and Low Dimensional Nanomaterials, School of Mathematics and Physics, North China Electric Power University, Beijing 102206, China

6 State Key Laboratory of Alternate Electrical Power System With Renewable Energy Sources, North China Electric Power University, Beijing 102206, China

7 Beijing Key Laboratory of Energy Safety and Clean Utilization, North China Electric Power University, Beijing 102206, China

substitute for this, the PCE of organic–inorganic hybrid perovskite solar cells has reached 25.2% [4, 5].

However, the poor stability of organic–inorganic hybrid perovskite ABX_3 (A^+ = organic cations; B^{2+} = inorganic cations; X^- = halide anions) seriously blocks its wide application. It has become a hot spot in both experiment and theory to clarify the degradation mechanism and improve the stability of organic–inorganic hybrid perovskites. A large number of studies have focused on screening ideal organic–inorganic hybrid perovskites with high environmental and structural stability [6–8]. $MAPbI_3$ was observed to be sensitive to the environment, especially to water, mainly because of the easy decomposition of PbI_3^- anion to PbI_2 in the presence of trace water [9]. However, due to the difficulty of experimental characterization, the decomposition mechanism remains unclear and even controversial [10]. Some have argued that one single water molecule could catalyze $MAPbI_3$ decomposition [11], whereas others proposed that decomposition does not occur unless more water molecules participate in the reaction [12]. Thanks to the development of DFT, Gao et al. [13] found that the stability of perovskites is highly dependent on the number of surrounding water molecules, and Tong et al. [14] concluded from the theory that one single H_2O molecule could hardly be adsorbed but would penetrate the $MAPbI_3$ internally causing instability. Obviously, compared to numerous experiments, DFT calculation presents an option to increase the understanding of perovskite stability at a molecular scale.

In the past, works paid enormous attention to the instability of ABX_3 caused by ambient atmosphere, UV light, and so on, whereas studies on the binding mechanism between A^+ and BX_3^- were relatively rare. In actuality, A^+ cations inside organic–inorganic hybrid perovskites are easy to volatilize [15], and researchers pointed out that the strong bindings between A^+ and BX_3^- are necessary for structural stability in that some observed that the desorption behavior of A^+ contributed to the formation of the vacancy on perovskite layers at the grain boundaries [16], and this might well be aroused from the inadequate formation energy of $A \cdots BX_3$ against the thermal drivers, which is in consistency with the insight of Wang et al. that the intrinsic binding mechanism is related to the structural stability, and the formation energy of corresponding molecular building blocks of the complexes $A \cdots BX_3$ could offer valuable information to quickly estimate the stability of the solar cell [17]. Until now, some have studied the binding mechanism of A^+ and BX_3^-, but the conclusions are different and variable. For instance, Fang et al. [18] stated that the binding was mainly from ionic bonding, but others reported that the binding strength arose from hydrogen bonding [17, 19]. Therefore, the binding mechanism between A^+ and BX_3^- needs to be clarified. Furthermore, a descriptor of the binding energy could provide guidance for highly stable organic–inorganic hybrid perovskites. As yet, this descriptor has not been proposed by prior work. Here, by using DFT, we explore the binding mechanism between A^+ and BX_3^-, with the work focused on two aspects. (1) Identify the origin of the binding strength between A^+ and BX_3^-. In this part, the ELF was plotted to study the orbital effect, the EDD map was utilized to explore the *Coulomb effect*, the RDG was used to determine inter-molecular interaction, and then EDA was made to clarify the energy composition of binding strength. (2) Propose a descriptor for binding strength based on the above analysis. We hope that this work can promote the comprehensive understanding of the internal binding mode inside organic–inorganic hybrid perovskite and contribute to the synthesis of perovskite-based solar materials with high structural stability in the future.

Calculation method

DFT was utilized for its high accuracy with relatively low computing cost [20–22]. All calculations in this work were performed at B3LYP[23]/def2SVP[24] level using the Gaussian 09 package [25]. The B3LYP functional has been proved to be rational for coincident results with CCSD(T) level for hybrid perovskites research [18]. Because of the large number of electrons in heavy atoms such as B site metal and I atoms, relativistic effective core potential of Stuttgart effective core potentials [26] was used to take into account the scalar relativistic effect, while spin–orbit coupling (SOC) was not considered since SOC was commonly ignored by previous works on binding interactions of similar cluster systems [27]. The def2-SVP basis set was selected and has been used extensively in prior perovskite studies [28–30]. Grimme's DFT-D3 method [31], which could increase calculating accuracy meanwhile saving computing resources, was used to correct dispersion interaction. The Multiwfn 3.7 code was used to perform wavefunction analysis [32].

Cluster models (CLMs) holding the same chemical ratio as those in bulk phases were built with the general chemical formula ABX_3. Compared with the periodic model, CLMs not only have lower computing costs, but also have benefits for analysis of the electronic structure due to their rich analytical information. By comparing with bulk phase model and known experimental data, the validation of CLMs has been clarified by previous studies. Fang et al. [18] investigated key structural features of hybrid perovskites using the same CLMs as these in this work and reported that the bond lengths in CLMs were the same as those obtained in a crystalline environment. They explored the LUMO–HOMO gap based on CLMs and found that though absolute values varied from those of band gaps in bulk phase models, the trends of two kinds of gaps were similar, and their relative variations were completely consistent [18]. Besides, $MAPbI_3$

degradation mechanism under trace water environment can be understood by CLMs [9]. More relevantly, Varadwaj et al. [33] further argued that inter-molecular interaction modes obtained from CLMs and bulk phase models should be aligned, and they reported that the optimized configurations using CLMs could perfectly explain reorientation phenomena of organic cation between perovskite faces, corners, and edges which had been observed by quasielastic neutron scattering and molecular dynamics simulation. Therefore, CLMs are suitable not only to describe geometry characteristics, but also to reveal intrinsic properties inside hybrid perovskites, and more detailed verification of CLMs with bulk phase models would be presented in the following parts of this work.

To evaluate the binding strength between the organic cation and anion, based on CLMs, the binding energy (E_b) of these two parts is calculated as follows [34, 35]: $E_b = E_{ABX3} - E_{A+} - E_{BX3}$-. Here, E_{ABX3}, E_{A+}, and E_{BX3}- are the electronic energies of the fully optimized perovskite, organic cation, and anion, respectively. In general, a more negative value of E_b corresponds to stronger interaction strength, and if the absolute value of E_b exceeds 0.5 eV, the two fragments would be bonded stably for chemisorption interaction [36, 37]. As an important fundamental of EDA, the total interaction energy (E_{toe}) between A^+ and BX_3^- was calculated. Here, the value of E_{toe} was directly obtained by subtracting the energies of the two fragments after electron relaxation from the energy of ABX_3. E_{toe} consists of two parts: the orbital interaction term (E_{orb}) and a summary of the electrostatic interaction term (E_{els}) as well as the exchange repulsion term (E_{ex}). For convenience, it is customary to combine E_{els} and E_{ex} terms in a steric term (E_{steric}). Because E_{ex} comes from the Pauli repulsion effect and is invariably positive, the value of E_{els} is always more negative than that of E_{steric}.

Results and discussion

Binding energy between A^+ and BX_3^-

Here, 36 CLMs of the most commonly typical organic–inorganic hybrid perovskites ($A^+ = CH_3NH_3^+$ (MA^+), $NH_2CHNH_2^+$ (FA^+), $CH_3CH_2NH_3^+$ (EA^+). $B^{2+} = Ge^{2+}$, Sn^{2+}, Pb^{2+}. $X^- = F^-$, Cl^-, Br^-, I^-) were set up, as shown in Fig. S1, to explore the binding mechanism between A^+ and BX_3^-. The small cluster used in this work shares the same chemical ratio and shows similar charge distribution as these models in the bulk phase, and thus it has been widely employed in previous studies on organic–inorganic hybrid perovskites [9, 17, 18, 38]. The calculation results such as binding energy and geometry parameters listed in Table S1 are consistent with not only prior published works but also the results from cubic bulk phase models in Figs. S2–S3, proving the accuracy of the calculations done in this research. It is noted that we compared the CLM with the tetragonal crystal structure of $MAPbI_3$ using the structural file provided in the literature [39] and found that there was a certain deviation between these models. For tetragonal structure, the shortest bond length between H and I atoms is 3.11 Å, while the distance in CLM and cubic structure is 2.56 and 2.64 Å, respectively. In addition, we calculated that the E_b between single MA and residual part of tetragonal $MAPbI_3$ is -4.10 eV, and this value is 0.63 and 0.61 eV lower than that in CLM (-4.73 eV) and cubic model (-4.71 eV), respectively. The E_b between single MA and residual part of tetragonal $MAPbBr_3$ and $MAPbCl_3$ is -5.18 and -4.44 eV, respectively. For $MAPbBr_3$, the binding of tetragonal phase nearly equals the values in CLM (-5.12 eV) and cubic phase (-5.32 eV). As for $MAPbCl_3$, the E_b in tetragonal phase is smaller by 1.07 and 0.85 eV, compared with these in CLM (-5.51 eV) and cubic model (-5.29 eV). In general, the trend of E_b is similar for cubic and tetragonal phase models, that is, I-contained components have the poor thermodynamic stability, while Br-contained perovskites is relatively outstanding. Therefore, it is concluded that with the exception of the Br-containing system, the binding energies of the three models decrease with increasing atomic number.

In this work, we optimized different adsorption configurations between MA^+ and BX_3^-, and the most stable configurations have been present in Fig. S1, with the less stable configurations shown in Fig. S2. We found that the most stable optimized structure is always the combination of -NH_3 and BX_3^-. To better understand this behavior, we carried out the electrostatic potential (ESP) analysis on the two fragments inside these CLMs, which has been widely used in previous works for the prediction of the most possible activity sites [40]. The X atom in ESP of BX_3^- is blue, as shown in Fig. 1, demonstrating that ESP of X atom is relatively negative, and thus the point where the A site organic cation contacts it should be the position where the electrostatic potential is relatively positive. Therefore, the ammonium moiety (-NH_3) in MA^+, double H atoms bonded to N atom in FA +, and -NH_3 in EA^+ should be the most possible sites to interact with BX_3^- due to the presentation of red ESP color, and this result could explain the calculating result of geometry configurations in Figs. S1–S2. It should be emphasized that the energy barrier between these stable configurations found at zero temperature can be easily overcome due to thermal effects and several different cation orientations can possibly be reached at room temperature [41]. Here, we only considered the most stable configurations as the research object in the following part.

The calculated E_b are all extremely large, suggesting that fierce interactions exist inside perovskites. Different A^+ and BX_3^- compositions lead to large binding energy

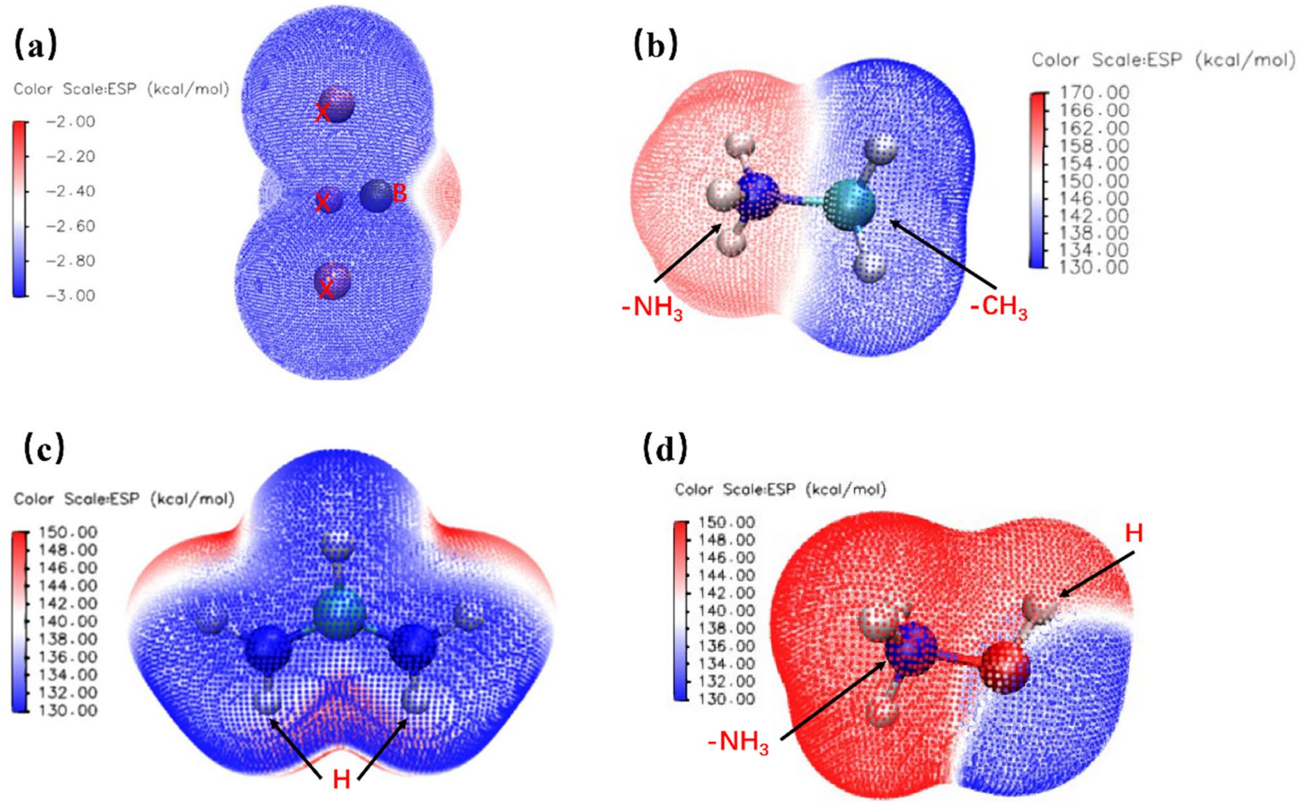

Fig. 1 Electrostatic potentials on the 0.001 e/Bohr^3 contour of BX_3^-(PbI_3^-), MA^+, FA^+, and EA^+. The values of electrostatic potential become increasingly negative from red to blue

discrimination. From Fig. 1, the different halogens showed significant influence on binding strength; that is, the values of E_b gradually declined in the order of F, Cl, Br, and I. Previous works have pointed out that some semi-empirical tolerance factors could well describe the structural stability of perovskites, among which the Goldschmidt tolerance factor (t) [42] and the octahedral tolerance factor (μ) [43] have become popular and widely employed. Based on Shannon ionic radius of A^+, B^{2+}, and X^- [44], the values of t and μ for CLMs in this study are calculated in Table S2. It is acknowledged that for values of t in the range of [0.78, 1.05] [45] or μ in the range of [0.414, 0.732] [46], perovskite compounds are expected to be generally stable, and we have highlighted these structures meeting the requirement of these tolerance factors in italics and bold. As for the researched perovskites, different structural descriptors lead to varying conclusions sometimes, suggesting that some new insights should be offered to deeply understand the stability of perovskites. In this work, E_b corresponds to the intrinsic interaction within molecular building modules and acts as a good supplement to the tolerance factors, and therefore it accounts to better understand the causes of high E_b and impacts of different halogens by adequate electronic structure exploration, which provides a new insight for structural stability of perovskites.

Electronic structure analysis

ELF was used to exhibit electronic localization properties on planes determined by H, halogen, and metal atoms, shown for MA-PbX_3 in Fig. 2. Red represents high electron localization area whereas blue means low electron localization area. In Fig. 2, the 1 *s* orbital of the H atom is obviously polarized to bond the N atom on MA^+, and halogen atom orbital polarization is weak. There is no obvious electronic localization area between the H and halogen atoms. Therefore, covalent effect is not the main source of high E_b. The electron cloud distribution of halogen atoms gradually diverges with the improvement of halogen atomic numbers, and this causes different charge distributions on MA-PbX_3. The calculated Hirshfeld atomic charge of marked H is + 0.12 e ($X = F^-$), + 0.11 e ($X = Cl^-$), + 0.11 e ($X = Br^-$), and + 0.11 e ($X = I^-$), and charge of X atom on PbX_3^- is − 0.37 e ($X = F^-$), − 0.34 e ($X = Cl^-$), − 0.32 e ($X = Br^-$), and − 0.31 e ($X = I^-$), respectively. According to the *Coulomb law*, the Coulomb attractive interaction between H and X would gradually decline. EDD maps (at 0.005 e/Å^3 intervals), from separate A^+ and BX_3^- fragments to complete ABX_3, are displayed in Fig. 3, where the yellow location represents the area gathering electrons

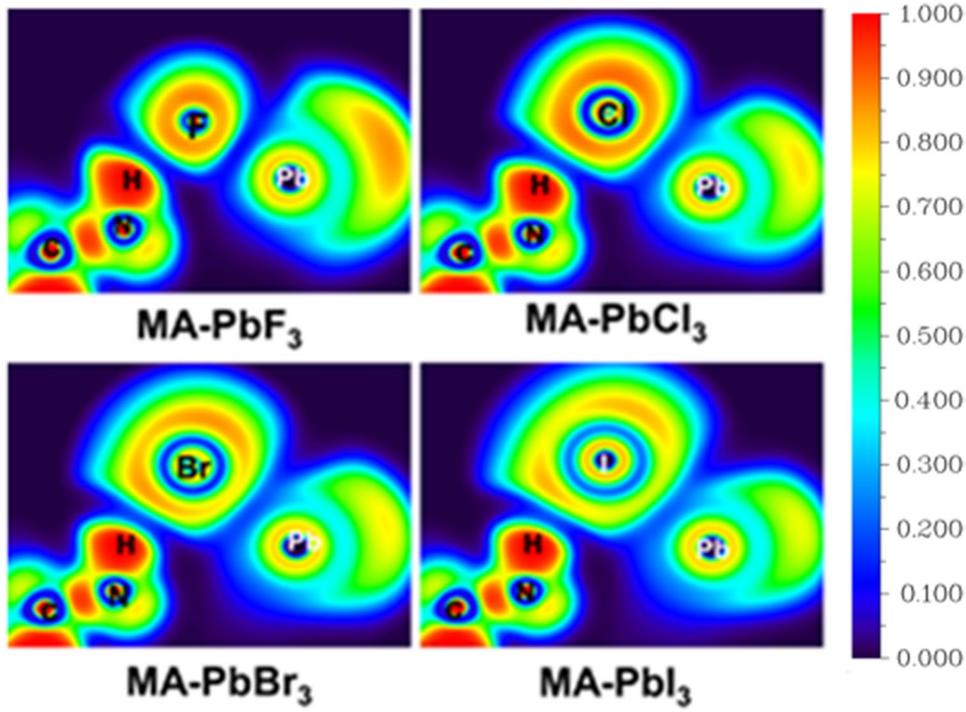

Fig. 2 ELF plot of MA-PbX_3 with X = F^-, Cl^-, Br^-, I^-

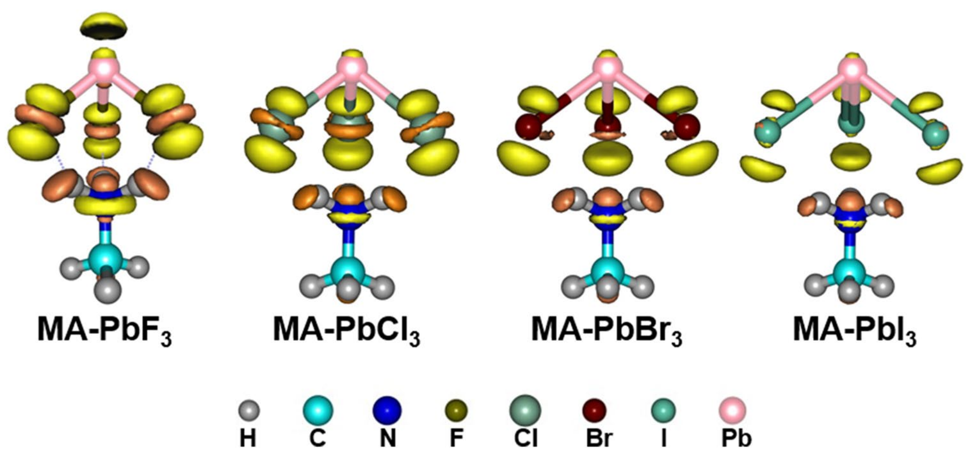

Fig. 3 EDD plot of MA-PbX_3 with X = F^-, Cl^-, Br^-, I^-

and the orange location represents the area losing electrons. It is found that the -NH_3 group rather than -CH_3 group is the main contributor to electron transfer in MA^+, additionally confirmed by first principles method using bulk phase models in others' works [47]. Consistent with the Hirshfeld charge result, the EDD maps prove that the charges accumulated on H and halogen atoms gradually decline. Therefore, we speculate that the fading E_b with changing of halogen atoms directly attributes to coulomb attraction force. To confirm our assumption, EDA was performed to obtain contributions of *Coulomb effect*, orbital effect, and weak interaction on binding strength.

According to the EDA result shown in Fig. 4, when both A^+ and B^{2+} are determined, E_{toe}, E_{orb}, and E_{steric} exhibit the same trend as E_b. It is obvious that both orbital energy and electrostatic energy impact the total interaction energy, but in comparison, the electrostatic energy makes the larger contribution. To distinguish who is the main contributor between *Coulomb effect* and weak interaction in electrostatic energy, RDG analysis was done (RDG = 0.5 a.u., electron density (ρ) < 0.05 a.u.), as shown in Fig. 5. The green area represents the weak interaction area. Hence, MA-PbI_3 has the strongest weak interaction, whereas MA-PbF_3 has the smallest weak interaction. Obviously, weak interaction strength order is thoroughly contrary to that of electrostatic energy with different X atoms. Therefore, the effect of weak interaction should be minor, and the *Coulomb effect* dominates the electrostatic energy and causes the large binding energy between MA^+ and PbI_3^-.

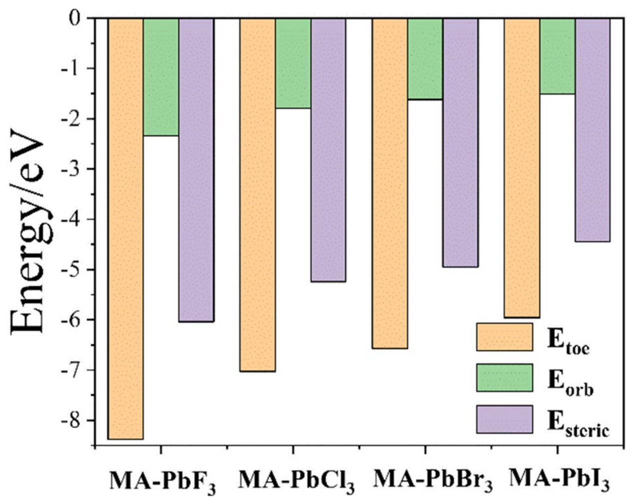

Fig. 4 EDA plot of MA-PbX_3 with X = F, Cl, Br, I

The electronic structure analysis was additionally confirmed by periodic bulk phase models, taking $MAPbX_3$ ($X = F^-$, Cl^-, Br^-, I^-) as an example and being shown in Figs. S3–S6 (for geometry, E_b, EDD, and projected density of states (PDOS) in bulk phase). The shortest bond lengths of H–X atoms were optimized to be 1.70 Å, 2.25 Å, 2.31 Å, and 2.64 Å in cubic ABX_3, extremely similar to these values in CLMs, being 1.66 Å, 2.16 Å, 2.32 Å, and 2.54 Å, respectively. The orientation of MA^+ is consistent between these two models that nitrogen atom faces the anion instead of the carbon atom, which may be due to the stronger electronegativity of the nitrogen atom. In addition, EDD plots of bulk phase models show the same trend as those of CLMs, as manifested by that accumulated electrons on X atoms are decreasing in the order of F, Cl, Br, and I, suggesting that the *Coulomb effect* is gradually fading. PDOS of bulk phase models revealed that there was no obvious orbital overlap between 1 *s* orbit of H and *p* orbit of X atoms near the fermi energy level, indicating that hybridization of H and X atoms was weak, and the covalent interaction should not very strong, which was also in agreement with the results from ELF analysis using CLMs. Therefore, the conclusion on electronic structure analysis obtained from CLMs should be the same as that from bulk phase models, and it is rational and reasonable, providing important fundamental as well as guidance for evaluating the binding strength between A^+ and BX_3^- in the following part.

Descriptor for binding energy between A^+ and BX_3^-

The above results, taking together with those in Figs. S7–S12 and Table S3 (for ELF, EDD, RDG, and EDA in CLMs), reveal that the *Coulomb effect* and orbital polarization are responsible for the large binding strength between A^+ and BX_3^-. However, the energy contributions in E_{toe} for different ABX_3 are varied. Figure S11 shows that for FA^+ cation, the main contribution to the binding energy is the orbital polarization, thus following opposite trends to MA^+ and EA^+, and this should attribute to that the huge charge transfer inside molecules can not only influence electrostatic interaction but also orbital term. To build an exact descriptor of the binding strength, an exploration of the effective independent variables representing these two energy compositions is needed. Inspired by *Coulomb law*, we defined Q^2/R_0 as an independent variable for the descriptor of E_b, where Q is the absolute value of the charge amount on A^+ and R_0 is the shortest bond length of linked A^+ and BX_3^-. Considering that the net charge on A^+ and BX_3^- is equal, Q^2/R_0 reflects the potential energy of the whole system. From Fig. 6, a linear relationship is evident between Q^2/R_0 and E_b with values of R^2 being 0.93 (MA-GeX_3), 0.98 (MA-SnX_3), 0.93 (MA-PbX_3), 0.97 (FA-GeX_3), 0.89 (FA-SnX_3), 0.75 (FA-PbX_3), 0.93 (EA-GeX_3), 0.98 (EA-SnX_3), and 0.997 (EA-PbX_3). All R^2 are near unity, suggesting that the *Coulomb effect* has a positive impact on binding and indicating that the energy contributed by the *Coulomb effect* with different X atoms is almost constant. Previous work has reported that the frontier orbitals energy gap of reactants directly corresponds to binding strength [48, 49], based on the Frontier Molecule Orbital (FMO) Theory. The net charge on A^+ inside a complete ABX_3 molecule was less than + 1 e, demonstrating that A^+ acts as an electron acceptor in the bonding process. Thus, we calculated the energy difference (E_{HL}) between LUMO of

Fig. 5 RDG plot of MA-PbX_3 with $X = F^-$, Cl^-, Br^-, I^-

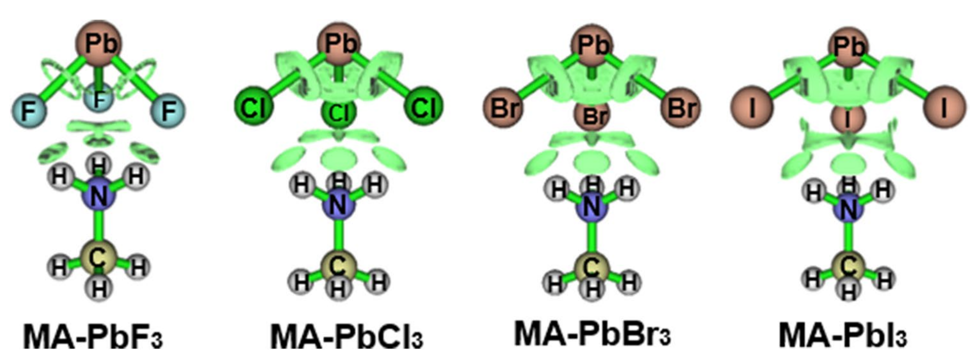

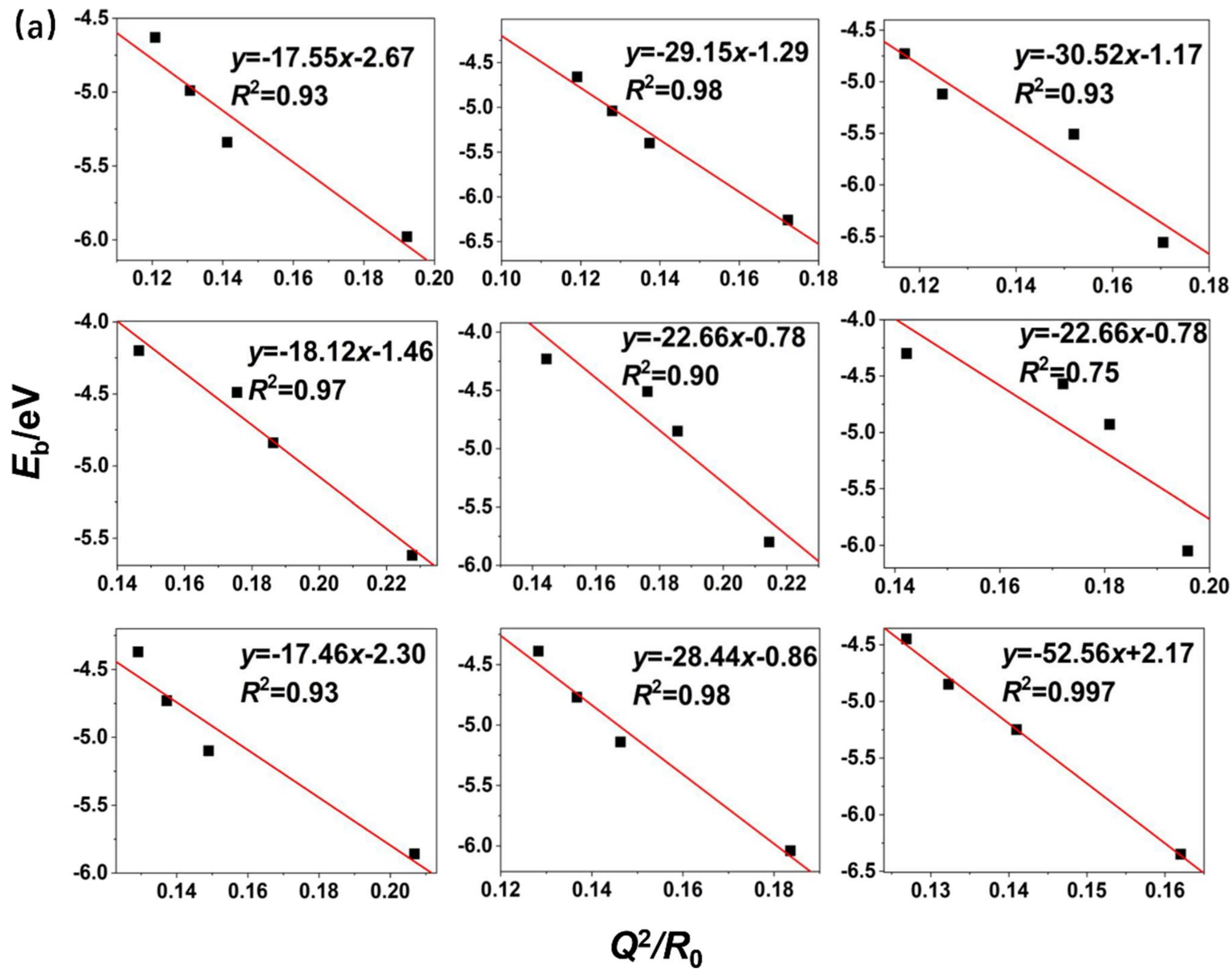

Fig. 6 Fitted lines between (**a**) Q^2/R_0 and E_b; (**b**) E_{HL} and E_b

A^+ and HOMO of BX_3^-. Linear relationships between E_{HL} as well as E_b were given, with high R^2 as 0.98 (MA-GeX_3), 0.995 (MA-SnX_3), 0.990 (MA-PbX_3), 0.999 (FA-GeX_3), 0.997 (FA-SnX_3), 0.998 (FA-PbX_3), 0.98 (EA-GeX_3), 0.998 (EA-SnX_3), and 0.98 (EA-PbX_3). Therefore, orbital effect participates in binding interactions and its contribution to the total interaction energy also almost remains unchanged with different halogens.

Although Q^2/R_0 and E_{HL} are descriptors for E_b, wide usage is limited given that those fitted equations are obviously different and lack universality. So, it is urgent to hunt for a more universal descriptor that not only describes E_b, but also covers more perovskites. Previous studies have reported that volume parameters influence chemical properties [50, 51] and that the molecular volume (V), as reflected by lattice constant in bulk phase model, can change properties of perovskites significantly. Taking both factors of energy contribution and molecular volume, in this work, we propose an effective binary descriptor with the E_b fitted against Q^2/R_0 and $V{\bullet}E_{HL}$ using the two-dimensional (2D) linear regression model shown in Fig. 7.

It can be seen from Fig. 7 that the data points of E_b are almost distributed around the fitting plane with $R^2=0.88$, proving that $E_b \sim (Q^2/R_0,\ V{\bullet}E_{HL})$ can be an effective descriptor for binding strength. The fitted equation is $E_b = -9.75(Q^2/R_0) + 0.00053\ (V{\bullet}E_{HL}) - 6.11$, which indicates that the larger is Q^2/R_0, and the smaller are V and E_{HL}, the more negative are the values of E_b (the units for Q, R_0, V, and E_{HL} are |e|, Å, bohr^3, and eV, respectively). For organic–inorganic hybrid perovskites, larger Q^2/R_0 is related to stronger energy arising from the *Coulomb effect*. Smaller V suggests tighter bindings, and lower E_{HL} means easier *FMO* interaction between HOMO of BX_3^- and LUMO of A^+. Therefore, this fitted equation is in accordance with the known *Coulomb law* and theory of *FMO*, confirming that the model of $E_b \sim (Q^2/R_0,\ V{\bullet}E_{HL})$ contains useful physical

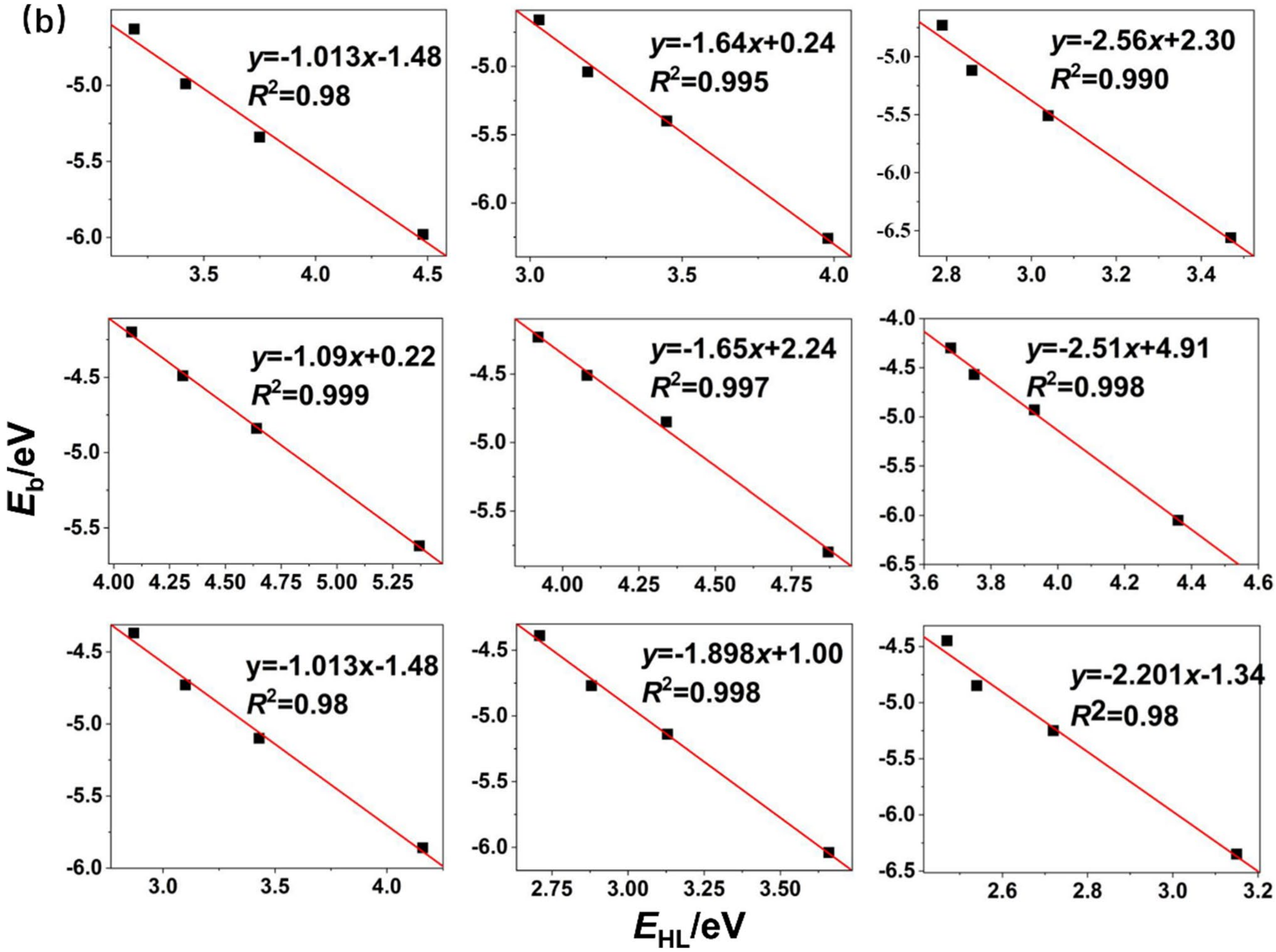

Fig. 6 (continued)

insights. We expect that this descriptor could effectively deepen the understanding of the binding mechanism of A^+ and BX_3^- within organic–inorganic hybrid perovskites, providing effective and rapid theoretical guidance for the design of perovskites with high stability. Moreover, based on the work, further research for the determinants of stability through the machine learning [52] and the ab initio molecular dynamics [53, 54] may be of great benefit to theoretical predictions of the structural stability of perovskites in the future.

Conclusions

Based on the electronic structures of 36 typical organic–inorganic perovskites CLMs, we have revealed the binding mechanism between A^+ and BX_3^-. The binding strength between the A^+ and BX_3^- acts as a descriptor to explain the link between the reduction of atomic number of X location and the enhancement of stability mentioned in the level of electronic structure. Though a certain difference between CLM and bulk is observed, this work reminds that some properties of organic–inorganic hybrid perovskites can be studied using cluster models, which will greatly improve the efficiency of high-throughput screening of stable perovskites furthermore. Besides, through analytical methods including ELF, EDD, RDG, and EDA, we found both the *Coulomb effect* and orbital effect impact the binding strength with each of their contributions being different. A novel 2D multiple linear regression descriptor was proposed between E_b and (Q^2/R_0, $V{\bullet}E_{HL}$) with coefficients of determination $R^2 = 0.88$. This descriptor provides guidance and a basis for the preparation of highly stable organic–inorganic hybrid perovskites in the future.

Supplementary Information The online version contains supplementary material available at https://doi.org/10.1007/s00894-022-05046-6.

Author contribution Xiaoshuo Liu: writing–original draft, investigation. Yang Bai: data curation, visualization. Shengyi Chen: formal analysis, investigation. ChongChong Wu: writing–review and editing.

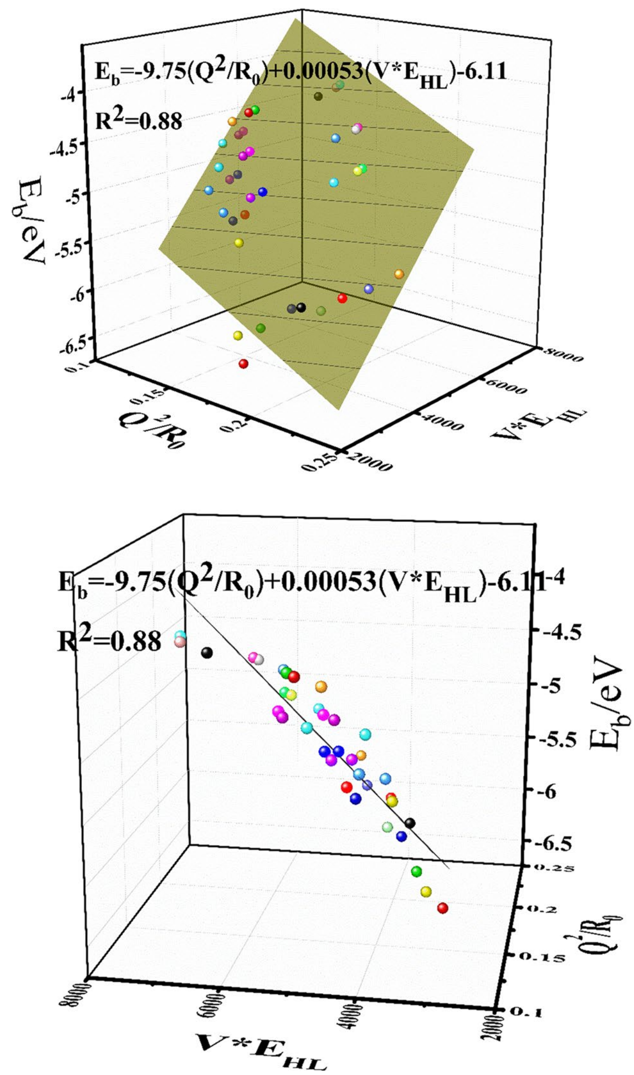

Fig. 7 Top and side views of fitted plane of $E_b \sim (Q^2/R_0, V \bullet E_{HL})$

Ian D. Gates: writing–review and editing. Tianfang Huang: validation. Weijie Yang: conceptualization, project administration. Wei Li: supervision. Zhengyang Gao: project administration, software. Jianxi Yao: project administration, funding acquisition. Xunlei Ding: project administration, writing– review and editing, software.

Funding This work was supported on National Key Research and Development Program of China (No. 2016YFA0202401), the National Natural Science Foundation of China (No. 52006073), the Beijing Natural Science Foundation (2182066), the Natural Science Foundation of Hebei Province of China (B2018502067 and E2020502023), and the Fundamental Research Funds for the Central Universities (2020MS104). CW and IDG acknowledge support from the University of Calgary's Canada First Research Excellence Fund program, the Global Research Initiative for Sustainable Low-Carbon Unconventional Resources.

Data availability The data used or analyzed during the current study are available on reasonable request.

Code available Not applicable.

Declarations

Ethics approval Not applicable.

Consent to participate Not applicable.

Consent for publication The authors confirmed that the work has not been published before, and it is not considered for others elsewhere. All authors agree to publication in the journal of *Journal of molecular modeling* after peer evaluation by Springer.

Conflict of interest The authors declare no competing interests.

References

1. Kojima A, Teshima K, Shirai Y, Miyasaka T (2009) Organometal halide perovskites as visible-light sensitizers for photovoltaic cells. J Am Chem Soc 131:6050–6051. https://doi.org/10.1021/ja809598r
2. Heo JH, Song DH, Han HJ, Kim SY, Kim JH, Kim D, Shin HW, Ahn TK, Wolf C, Lee TW (2015) Planar CH3NH3PbI3 perovskite solar cells with constant 17.2% average power conversion efficiency irrespective of the scan rate. Adv Mater. 27:3424–3430. https://doi.org/10.1002/adma.201500048
3. Kowalczewski P, Andreani LC (2015) Towards the efficiency limits of silicon solar cells: how thin is too thin? Sol Energy Mater Sol Cells 143:260–268. https://doi.org/10.1016/j.solmat.2015.06.054
4. You S, Xi X, Zhang X, Wang H, Gao P, Ma X, Bi S, Zhang J, Zhou H, Wei Z (2020) Long-term stable and highly efficient perovskite solar cells with a formamidinium chloride (FACl) additive. J Mater Chem A 8:17756–17764. https://doi.org/10.1039/D0TA05676F
5. Arias-Ramos CF, Kumar Y, Abrego-Martínez PG, Hu H (2020) Efficient and stable hybrid perovskite prepared at 60% relative humidity with a hydrophobic additive in anti-solvent. Sol Energy Mater Sol Cells 215:110625. https://doi.org/10.1016/j.solmat.202020.110625
6. Lu S, Zhou Q, Ouyang Y, Guo Y, Li Q, Wang J (2018) Accelerated discovery of stable lead-free hybrid organic-inorganic perovskites via machine learning. Nat Commun 9:3405. https://doi.org/10.1038/s41467-018-05761-w
7. Lim J, Kim M, Park HH, Jung H, Lim S, Hao X, Choi E, Park S, Lee M, Liu Z, Green MA, Seo J, Park J, Yun JS (2021) Kinetics of light-induced degradation in semi-transparent perovskite solar cells. Sol Energy Mater Sol Cells 219:110776. https://doi.org/10.1016/j.solmat.2020.110776
8. Xia J, Luo J, Yang H, Wan Z, Malik HA, Shi Y, Yao X, Jia C (2020) Interface induced in-situ vertical phase separation from $MAPbI_3$:Spiro-OMeTAD precursors for perovskite solar cells. Sol Energy Mater Sol Cells 216:110689. https://doi.org/10.1016/j.solmat.2020.110689
9. Fang H, Jena P (2017) Atomic-level design of water-resistant hybrid perovskites for solar cells by using cluster ions. J Phys Chem Lett 8:3726–3733. https://doi.org/10.1021/acs.jpclett.7b01529
10. Zhu Z, Hadjiev VG, Rong Y, Guo R, Cao B, Tang Z, Qin F, Li Y, Wang Y, Hao F, Venkatesan S, Li W, Baldelli S, Guloy AM, Fang H, Hu Y, Yao Y, Wang Z, Bao J (2016) Interaction of organic cation with water molecule in perovskite $MAPbI_3$: From

dynamic orientational disorder to hydrogen bonding. Chem Mater 28:7385–7393. https://doi.org/10.1021/acs.chemmater.6b02883

11. Niu G, Guo X, Wang L (2015) Review of recent progress in chemical stability of perovskite solar cells. J Mater Chem A 3:8970–8980. https://doi.org/10.1039/C4TA04994B
12 Christians JA, Miranda Herrera PA, Kamat PV (2015) Transformation of the excited state and photovoltaic efficiency of $CH_3NH_3PbI_3$ perovskite upon controlled exposure to humidified air. J Am Chem Soc. 137:1530–1538. https://doi.org/10.1021/ja511132a
13. Gao Z, Yan G, Zhao M, Xu S, Li L, Huang H, Yang W, Ding X (2019) Theoretical insights into the stability of perovskite clusters by studying water adsorption on $(CH_3NH_3)_4SnI_6$. Sol Energy Mater Sol Cells 202:110126. https://doi.org/10.1016/j.solmat.2019.110126
14. Tong C-J, Geng W, Tang Z-K, Yam C-Y, Fan X-L, Liu J, Lau W-M, Liu L-M (2015) Uncovering the veil of the degradation in perovskite $CH_3NH_3PbI_3$ upon humidity exposure: a first-principles study. J Phys Chem Lett 6:3289–3295. https://doi.org/10.1021/acs.jpclett.5b01544
15. Li B, Ferguson V, Silva SRP, Zhang W (2018) Defect engineering toward highly efficient and stable perovskite solar cells. Adv Mater Interfaces 5:1800326. https://doi.org/10.1002/admi.201800326
16. Ranjan R, Usmani B, Pali S, Ranjan S, Singh A, Garg A, Gupta RK (2020) Role of PC60BM in defect passivation and improving degradation behaviour in planar perovskite solar cells. Sol Energy Mater Sol Cells 207:110335. https://doi.org/10.1016/j.solmat.2019.110335
17. Wang M, Li W, Lu F, Ding X (2020) Theoretical study on the stability of the complexes A...BX_3 [A = CH_3NH_3(+), NH_2CHNH_2(+), NH_2CHOH(+); B = Sn(2+), Pb(2+); X = F(-), Cl(-), Br(-), I(-)]. J Mol Model 26: 46. https://doi.org/10.1007/s00894-020-4303-1.
18. Fang H, Jena P (2016) Molecular origin of properties of organic-inorganic hybrid perovskites: the big picture from small clusters. J Phys Chem Lett 7:1596–1603. https://doi.org/10.1021/acs.jpclett.6b00435
19. Ghosh D, Smith AR, Walker AB, Islam MS (2018) Mixed A-cation perovskites for solar cells: Atomic-scale insights into structural distortion, hydrogen bonding, and electronic properties. Chem Mater 30:5194–5204. https://doi.org/10.1021/acs.chemmater.8b01851
20. Li H, Guo S, Shin K, Wong MS, Henkelman G (2019) Design of a Pd–Au nitrite reduction catalyst by identifying and optimizing active ensembles. ACS Catal 9:7957–7966. https://doi.org/10.1021/acscatal.9b02182
21. Li H, Shin K, Henkelman G (2018) Effects of ensembles, ligand, and strain on adsorbate binding to alloy surfaces. J Chem Phys 149:174705. https://doi.org/10.1063/1.5053894
22. Liu C, Li H, Liu F, Chen J, Yu Z, Yuan Z, Wang C, Zheng H, Henkelman G, Wei L, Chen Y (2020) Intrinsic activity of metal centers in metal-nitrogen-carbon single-atom catalysts for hydrogen peroxide synthesis, J Am Chem Soc 21861–21871. https://doi.org/10.1021/jacs.0c10636.
23. Stephens PJ, Devlin FJ, Chabalowski CF, Frisch MJ (1994) Ab initio calculation of vibrational absorption and circular dichroism spectra using density functional force fields. J Chem Phys 98:11623–11627. https://doi.org/10.1021/j100096a001
24. Weigend F, Ahlrichs R (2005) Balanced basis sets of split valence, triple zeta valence and quadruple zeta valence quality for H to Rn: Design and assessment of accuracy. Phys Chem Chem Phys 7:3297–3305. https://doi.org/10.1039/B508541A
25. Frisch MJ, Trucks GW, Schlegel HB, Scuseria GE, Robb MA, Cheeseman JR, Scalmani G, Barone V, Petersson GA, Nakatsuji H, Li X, Caricato M, Marenich A, Bloino J, Janesko BG, Gomperts R, Mennucci B, Hratchian HP, Ortiz JV, Izmaylov AF, Sonnenberg JL, Williams-Young D, Ding F, Lipparini F, Egidi F, Goings J, Peng B, Petrone A, Henderson T, Ranasinghe D, Zakrzewski VG, Gao J, Rega N, Zheng G, Liang W, Hada M, Ehara M, Toyota K, Fukuda R, Hasegawa J, Ishida M, Nakajima T, Honda Y, Kitao O, Nakai H, Vreven T, Throssell K, Montgomery J. A, Jr, Peralta JE, Ogliaro F, Bearpark M, Heyd JJ, Brothers E, Kudin KN, Staroverov VN, Keith T, Kobayashi R, Normand J, Raghavachari K, Rendell A, Burant JC, Iyengar SS, Tomasi J, Cossi M, Millam JM, Klene M, Adamo C, Cammi R, Ochterski JW, Martin RL, Morokuma K, Farkas O, Foresman JB, Fox DJ (2009) Gaussian 09, Revision D.01, Gaussian, Inc., Wallingford CT.
26. Matczak P (2017) Description of weak halogen bonding using various levels of symmetry-adapted perturbation theory combined with effective core potentials. J Chem 2017:9031494. https://doi.org/10.1155/2017/9031494
27. Xie N, Wang H, You C (2021) Role of oxygen functional groups in Pb^{2+} adsorption from aqueous solution on carbonaceous surface: A density functional theory study. J Hazard Mater 405:124221. https://doi.org/10.1016/j.jhazmat.2020.124221
28. Lu H, He B, Ji Y, Shan Y, Zhong C, Xu J, LiuYang J, Wu F, Zhu L (2020) Dopant-free hole transport materials processed with green solvent for efficient perovskite solar cells. Chem Eng J 385:123976. https://doi.org/10.1016/j.cej.2019.123976
29. Magomedov A, Kasparavičius E, Rakstys K, Paek S, Gasilova N, Genevičius K, Juška G, Malinauskas T, Nazeeruddin MK, Getautis V (2018) Pyridination of hole transporting material in perovskite solar cells questions the long-term stability. J Mater Chem C 6:8874–8878. https://doi.org/10.1039/C8TC02242A
30. Yang Y, Wu F, Lu H, Li S, Zhong C, Zhu L (2020) Bipyrimidine core structure-based hole transport materials for efficient perovskite solar cells, Sustain. Energy Fuels 4:5271–5276. https://doi.org/10.1039/D0SE01062F
31. Grimme S, Antony J, Ehrlich S, Krieg H (2010) A consistent and accurate ab initio parametrization of density functional dispersion correction (DFT-D) for the 94 elements H-Pu. J Chem Phys 132:154104. https://doi.org/10.1063/1.3382344
32. Lu T, Chen F (2012) Multiwfn: a multifunctional wavefunction analyzer. J Comput Chem 33:580–592. https://doi.org/10.1002/jcc.22885
33. Varadwaj A, Varadwaj PR, Yamashita K (2017) Hybrid organic-inorganic $CH_3NH_3PbI_3$ perovskite building blocks: Revealing ultra-strong hydrogen bonding and mulliken inner complexes and their implications in materials design. J Comput Chem 38:2802–2818. https://doi.org/10.1002/jcc.25073
34. Liu X, Gao Z, Wang C, Zhao M, Ding X, Yang W, Ding Z (2019) Hg^0 oxidation and SO_3, Pb^0, PbO, $PbCl_2$ and As_2O_3 adsorption by graphene-based bimetallic catalyst ((Fe, Co)@N-GN): A DFT study. Appl Surf Sci 496:143686. https://doi.org/10.1016/j.apsusc.2019.143686
35. Liu X, Gao Z, Huang H, Yan G, Huang T, Chen C, Yang W, Ding X-L (2020) Simultaneous catalytic oxidation of nitric oxide and elemental mercury by single-atom Pd/g-C_3N_4 catalyst: A DFT study. Mol Catal 488:110901. https://doi.org/10.1016/j.mcat.2020.110901
36. Gao Z, Zhao M, Yan G, Huang H, Yang W, Ding X, Wu C, Gates ID (2020) Identifying the active sites of carbonaceous surface for the adsorption of gaseous arsenic trioxide: A theoretical study. Chem Eng J. 402:125800. https://doi.org/10.1016/j.cej.2020.125800
37. Gao Z, Liu X, Li A, Ma C, Li X, Ding X, Yang W (2019) Adsorption behavior of mercuric oxide clusters on activated carbon and the effect of SO_2 on this adsorption: a theoretical investigation. J Mol Model 25:142. https://doi.org/10.1007/s00894-019-4026-3

38. Fang H, Jena P (2016) Super-ion inspired colorful hybrid perovskite solar cells. J Mater Chem A 4:4728–4737. https://doi.org/10.1039/C5TA09646D
39. Frohna K, Deshpande T, Harter J, Peng W, Barker BA, Neaton JB, Louie SG, Bakr OM, Hsieh D, Bernardi M (2018) Inversion symmetry and bulk Rashba effect in methylammonium lead iodide perovskite single crystals. Nat Commun 9:1829. https://doi.org/10.1038/s41467-018-04212-w
40. Gao Z, Ding Y (2017) DFT study of CO_2 and H_2O co-adsorption on carbon models of coal surface. J Mol Model 23:187. https://doi.org/10.1007/s00894-017-3356-2
41. Quarti C, Mosconi E, De Angelis F (2014) Interplay of orientational order and electronic structure in methylammonium lead iodide: implications for solar cell operation. Chem Mater 26:6557–6569. https://doi.org/10.1021/cm5032046
42. Goldschmidt VM (1926) Die gesetze der krystallochemie. Naturwissenschaften 14:477–485. https://doi.org/10.1007/BF01507527
43. Travis W, Glover ENK, Bronstein H, Scanlon DO, Palgrave RG (2016) On the application of the tolerance factor to inorganic and hybrid halide perovskites: a revised system. Chem Sci 7:4548–4556. https://doi.org/10.1039/C5SC04845A
44. Shanno RD (1976) Revised effective ionic radii and systematic studies of interatomic distances in halides and chalcogenides. Acta Cryst A 32:751–767. https://doi.org/10.1107/S0567739476001551
45. Gao Z, Chen S, Bai Y, Wang M, Liu X, Yang W, Li W, Ding X, Yao J (2021) A new perspective for evaluating the photoelectric performance of organic–inorganic hybrid perovskites based on the DFT calculations of excited states. Phys Chem Chem Phys 23:11548–11556. https://doi.org/10.1039/D1CP01000J
46. Shi T, Li G, Zhu J (2017) Compositional design strategy for high performance ferroelectric oxides with perovskite structure. Ceram Int 43:2910–2917. https://doi.org/10.1016/j.ceramint.2016.11.085
47. Becker M, Kluner T, Wark M (2017) Formation of hybrid ABX_3 perovskite compounds for solar cell application: first-principles calculations of effective ionic radii and determination of tolerance factors. Dalton Trans 46:3500–3509. https://doi.org/10.1039/C6DT04796C
48. Gao Z-Y, Yang W-J, Ding X-L, Lv G, Yan W-P (2018) Support effects on adsorption and catalytic activation of O_2 in single atom iron catalysts with graphene-based substrates. Phys Chem Chem Phys 20:7333–7341. https://doi.org/10.1039/C7CP08301G
49. Ling Y, Wu J, Li B, Liu D (2021) Insights into the mechanism of elemental mercury adsorption on graphitic carbon nitride: a density functional theory study. Energy Fuels 35:9322–9331. https://doi.org/10.1021/acs.energyfuels.1c00624
50. Li H, Xu S, Wang M, Chen Z, Ji F, Cheng K, Gao Z, Ding Z, Yang W (2020) Computational design of (100) alloy surfaces for the hydrogen evolution reaction. J Mater Chem A 8:17987–17997. https://doi.org/10.1039/D0TA04615A
51. Li H, Zhang Z, Liu Z (2019) Non-monotonic trends of hydrogen adsorption on single atom doped g-C_3N_4. Catalysts 9:84. https://doi.org/10.3390/catal9010084
52. Gao Z, Zhang H, Mao G, Ren J, Chen Z, Wu C, Gates ID, Yang W, Ding X, Yao J (2021) Appl Surf Sci 561:150916. https://doi.org/10.1016/j.apsusc.2021.150916
53. Yang L, Chen Y, Wang X, Deng J, Wang W, Ding X, Yang W, Yao J (2021) J Phys Chem C 125(43):24096–24104. https://doi.org/10.1021/acs.jpcc.1c06317
54. Gao Z, Wang M, Zhang H, Chen S, Wu C, Gates ID, Yang W, Ding X, Yao J (2021) Sol Energy Mater Sol Cells 233:111401. https://doi.org/10.1016/j.solmat.2021.111401